# Terahertz Radiation from a Photoconducting Antenna Array

Nan M. Froberg, Bin Bin Hu, Xi-Cheng Zhang, and David H. Auston, *Fellow, IEEE*

*Invited Paper*

***Abstract*—We describe an array of photoconducting antennas which generates electrically controllable millimeter wave and submillimeter wave radiation in free space. Under quasi-sinusoidal optical illumination, the emitted radiation is directional and electrically steerable, and can be scanned through an angle of over 40°. The center of the scanning range can be adjusted by changing the angle of incidence of the pump beam. The far-field radiation pattern of the array is measured and discussed. Also, some properties of the array under illumination by a short optical pulse are demonstrated. These include electrical control of the frequency content of the signal, and mapping of the spatial profile of the applied electric field onto the radiated waveform. The latter property can be used to multiplex information presented in parallel into a train of radiated pulses with a bit spacing of 6 ps.**

## I. Introduction

OVER the last decade, various techniques have been developed to generate and detect extremely short pulses of electromagnetic radiation in free space. With the exception of electrooptic Cherenkov radiation [1], the emitters generally use a photoconductive material to create a radiative current transient, and are known as photoconducting antennas. In early devices, the photoconductor was integrated into a waveguide or transmission line, and when illuminated by a short optical pulse, produced a short electrical pulse which drove a nearby antenna [2], [3]. Later on, the photoconducting material was integrated directly into the antenna structure to eliminate distortion and broadening of the electrical pulse in transit [4]. Photoconducting versions of Hertzian dipoles [4], tapered slotline and stripline antennas [3], [5], [6], dipole antennas [7], [8], and spiral antennas [9], [10] have been reported. However, very simple structures can also serve as emitters, since all that is needed to generate a current transient is a photoconductor which is subjected to an electric field and illuminated by a short optical pulse. Such a source can be made by depositing a pair of electrodes on a semiconductor, applying a voltage and illuminating all or part of the gap [11]–[13]. Even more simply, the surface depletion field of the semiconductor can serve as the dc bias field which drives the transient current, eliminating the need for electrodes [14]. A reverse-biased p–i–n diode is also a strong source of radiation [15].

The free-space electrical pulses generated by photoconducting antennas can be extremely fast, with spectral content ranging from a few GHz to over 4 THz [16]. If a fast photoconductor such as a radiation-damaged semiconductor is used in the antenna, it can also function as a sensitive and phase-coherent detector [4]. With the addition of terahertz optics to collect and collimate the beam [17], an emitter/detector pair of photoconducting antennas provides a powerful spectroscopic system for measuring the absorption and dispersion of materials. This system has been used to characterize dielectrics [18], [19], semiconductors [19]–[21], coupled quantum wells [22], and superconductors [23], [24] in the millimeter to submillimeter wave region of the spectrum. The time dependence of optical carrier injection has also been studied using this method [2], [25]. Finally, the radiated waveform has been analyzed to provide information about internal fields [14], [26] and nonlinear effects [27] in the emitter.

Photoconducting antennas have proven their usefulness in the characterization of materials, and as they continue to develop, their ability to produce nearly single-cycle pulses of millimeter-wave radiation may be relevant to other areas. One possible application is radar. Recently, optics has played a significant role in phased array radar research [28]. Signal distribution via optical fiber provides advantages in increased bandwidth, low attenuation and reduction of system size and weight [29]. Optical generation of microwave signals via heterodyning techniques and optoelectronic methods of phase control have also been demonstrated. In early work on photoconducting antennas, it was pointed out that the pulsed nature of photoconducting antennas would lend itself to high resolution time-resolved radar systems [2], [3]. Mourou *et al.* [2] demonstrated a simple radar system using an aluminum target to reflect the microwave pulses back to a detector; the target position was determined by the time delay of the echo.

Many radar applications would require a directional and scannable beam. Photoconducting antennas in which the

Manuscript received February 28, 1992; revised May 21, 1992. This work was supported by the National Center for Integrated Photonic Technology. The work of N. M. Froberg was supported by an IBM Fellowship.

N. M. Froberg, B. B. Hu, and D. H. Auston are with the Department of Electrical Engineering, Columbia University, New York, NY, 10027.

X.-C. Zhang was with the Department of Electrical Engineering, Columbia University, New York, NY 10027. He is now with the Department of Physics, Rensselaer Polytechnic Institute, Troy, NY 12180.

IEEE Log Number 9202063.

0018-9197/92$03.00 © 1992 IEEE

emitting aperture is large compared to the radiated wavelength have been shown to produce diffraction-limited and optically steerable radiation [12]. However, optical control of the beam direction is relatively difficult and slow. It would be preferable to steer the beam electrically via the traditional method of an antenna array. A phased array of photoconducting antennas, fed by a fiber bundle, was proposed but not demonstrated in the early 1980's [3].

Recently, we have pursued this concept experimentally, by fabricating and characterizing a photoconducting antenna array in which the amplitude of each antenna element, rather than the phase, can be independently controlled [30]–[32]. This array is formed by a pattern of parallel electrodes deposited on semiinsulating GaAs. The photoconducting gap between each pair of adjacent electrodes forms a single antenna element. When a subpicosecond laser pulse illuminates the structure, each element emits a broad-band electromagnetic pulse, the amplitude of which is proportional to the electric field between the electrodes. Consequently, the strength of each emitter can be controlled by biasing the electrodes appropriately.

We have demonstrated that a photoconducting antenna array can produce a directional and electrically steerable submillimeter wave beam [30]. This is accomplished by biasing the elements so that their amplitudes vary sinusoidally as a function of their position in the array. As the period of the sinusoidal bias is varied, the emitted beam changes direction. The angle into which the emitted radiation will be steered is also a function of wavelength; therefore, only a relatively narrow-band signal can be electrically scanned in this way. To reduce the spectral content of the normally broad-band radiation emitted by the antenna elements, the array was pumped with quasi-sinusoidal optical modulation. The signal component at 480 GHz was electrically scanned over 30°, and had a full width at half maximum between 6 and 9°. The scanning angle and directionality of the beam could be increased by increasing the element density and the overall length.

Although the steering property of the array requires narrow-band radiation, the array has several interesting functions when it is illuminated by a single short optical pulse and is radiating nondirectional broad-band electrical pulses. If a sinusoidal bias pattern is applied to the electrodes as in the steering experiment, the frequency content of the radiation emitted in a given direction can be electrically controlled [31]. This frequency tuning is made possible by the same principles as the electrical steering: the array acts like a programmable grating, in which the effective grating spacing is determined by the applied electric field. We have scanned the peak signal frequency from 200 to 800 GHz, and this range could be easily extended by modifications to the device.

Finally, the array has some interesting properties relating to the time dependence of the emitted pulse rather than the radiation pattern. Under single pulse illumination, the spatial profile of the bias field applied to the array is mapped on to the temporal profile of the radiated waveform [32]. Consequently, the array can be used as a multiplexer, where zeros and ones encoded onto the spatial bias field in parallel are converted to a sequential series of zeros and ones in the radiated waveform. We have generated a four-bit word in which the spacing between bits is about 6 ps, corresponding to 170 GHz.

The first section of the paper discusses the application of antenna theory to photoconducting antennas. Next, the steering properties of the array are presented theoretically and experimentally. Finally, the frequency tuning and spatial-to-temporal mapping properties are explored. In the discussion we will mention some future directions for research.

## II. Array Theory for Photoconducting Antennas

The principles of scanning an electromagnetic wave by means of an antenna array are well known from traditional antenna theory [33], and require only a few modifications to be applied to photoconducting devices. The setup is shown schematically in Fig. 1. The $z$ axis is defined in the plane of the wafer, perpendicular to the electrodes. Thus, the emitting elements, which consist of the photoconducting gaps between each adjacent pair of electrodes, are distributed along the $z$ axis and are oriented in the $z$ direction. Assuming that these elements can be modeled as short electric dipoles, the radiated field in the far-field limit is given by

$$E_\theta(\vec{r}, t) = \frac{\mu_o}{4\pi r} \cos\theta \frac{\partial}{\partial t} \cdot \left[ \sum_{n=1}^{N} J_n \left( z_n, t - t_n - \frac{|\vec{r} - \vec{r}_n|}{c} \right) A \right] \tag{1}$$

where $\mu_o$ is the permeability of free space, $\vec{r}$ is the detection point, $\theta$ is the angle of detection with respect to the array normal, $J_n$, $z_n$, $\vec{r}_n$, and $t_n$ are the surface current density, $z$-coordinate, position vector and time of radiation of the $n$th array element, respectively, $N$ is the total number of elements, $A$ is the emitting area of each element, $c$ is the speed of light, and the position coordinates are defined relative to the array center. It is assumed below that the detection point is in the plane of incidence, and that $z_n << r$ for all elements. Then the delay caused by the path difference from the $n$th element to the detection point is

$$\delta \left[ \frac{|\vec{r} - \vec{r}_n|}{c} \right] = \frac{nd \sin\theta}{c} \tag{2}$$

where $d$ is the spacing between elements. If the optical beam is incident on the array at an angle $\alpha$ with respect to the normal, the time delay before radiation of an element is given by

$$\delta t_n = nd \sin\alpha / c. \tag{3}$$

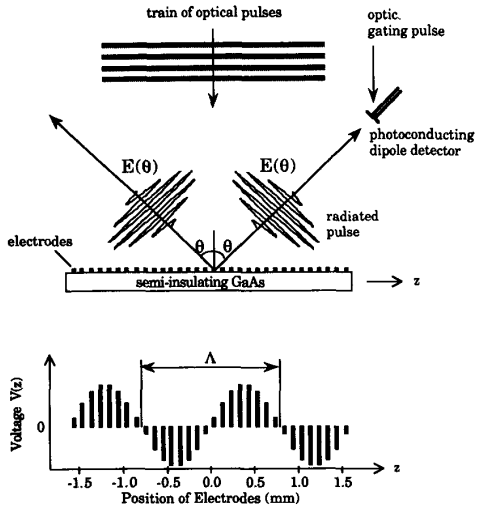


Fig. 1. Setup for the generation of an electrically steerable submillimeter wave beam. The array electrodes are sinusoidally biased with respect to their position, as shown. The array is illuminated with a train of optical pulses in order to generate quasi-sinusoidal radiation.

Substituting (2) and (3) into (1) gives

$$E_\theta(r, \theta, t) = \frac{\mu_0}{4\pi r} A \cos\theta \cdot \frac{\partial}{\partial t} \sum_{n=1}^{N} J_n\left(z_n, t - \frac{nd}{c}(\sin\theta + \sin\alpha)\right). \tag{4}$$

Some approximations must be made about the field and time dependence of the photocurrent elements $J_n$ in GaAs under illumination by a subpicosecond pulse. While we have implied above that the radiation results from a real photocurrent, optically induced radiation has also been attributed to optical rectification [34]. Since the details of the radiation process are not crucial to the operation of the array, we will use a very simple model for the real photocurrent to illustrate some basic dependences. It has been found experimentally that the far-field radiation from an antenna scales with the applied field for the field strengths of interest, which are a few kV/cm. Therefore we use the following expression for the photocurrent:

$$J_n(\vec{r}_n, t) \approx \sigma_s(t) E_b(z_n) = \sigma_s(t) E_{bn}. \tag{5}$$

Combining (4) and (5) gives

$$E_\theta(r, \theta, t) = \frac{\mu_0}{4\pi r} A \cos\theta \cdot \sum_{n=1}^{N} E_{bn} \frac{\partial}{\partial t} \sigma_s\left(t - \frac{nd}{c}(\sin\theta + \sin\alpha)\right). \tag{6}$$

If the carriers responded instantly to the field, the photoconductivity would be proportional to the carrier density, and its first derivative would follow the Gaussian envelope of the optical pulse. In the case of optical rectification [34], which is very fast, this assumption would be justified. For a real photocurrent, however, Monte-Carlo calculations show that the rise time may vary from a few hundred femtoseconds to a few picoseconds, depending on the ratio of the initial photon energy to the steady-state energy supplied by the field [35]. We will assume that the time derivative of the photoconductivity is a Gaussian, but use a time constant longer than the optical pulse width to account for the rise time of the carrier velocity. The radiation strength should be proportional to an average transient mobility $\mu_{\text{trans}}$, and to the sheet carrier density $N_s$ injected by the optical pulse:

$$\frac{\partial \sigma_s}{\partial t} \approx \frac{\partial}{dt}[n_s(t) e\mu(t)] \approx e\mu_{\text{trans}} N_s F_s(t) \approx e\mu_{\text{trans}} \frac{(1 - R) W_{\text{opt}}}{h\upsilon} F_s(t, \tau_o). \tag{7}$$

Here $R$ is the reflectivity of the photoconductor, $W_{opt}$ is the energy density of the optical pulse, $\upsilon$ is the optical frequency, and $F_s(t, \tau_o)$ is a Gaussian function with pulsewidth $\tau_o$, normalized to have unit area. This approximation is only valid during the rise time of the pulse when the radiation occurs; the photocurrent decay is by recombination and is too slow to contribute much to the radiative process.

In the next sections, it will be easier to work in the frequency domain. Combining (6) and (7) and transforming gives

$$E_\theta(\omega) = \frac{\mu_0 A \cos\theta}{4\pi r} \frac{e\mu_{\text{trans}}(1 - R) W_{\text{opt}}}{h\upsilon} \cdot \sum_{n=1}^{N} E_{bn} F_s(\omega, \tau_o) e^{-jknd(\sin\theta + \sin\alpha)} \tag{8}$$

where $E_\theta(\omega)$ and $F_s(\omega, \tau_o)$ are the Fourier components of the radiated field and the normalized Gaussian, respectively, and $k = 2\pi/\lambda$ is the wavenumber of the free-space radiation.

## III. Electrical Scanning of 500 GHz Radiation

### A. Theory

In order to steer the emitted beam, a sinusoidal voltage bias with period $\Lambda_{\text{bias}}$ is applied to the electrodes as shown in Fig. 1. The field applied to an antenna element is then

$$E_n = -\left.\frac{\partial V(z)}{\partial z}\right|_{z = z_n} \approx E_{b0} \sin(n\kappa d) \tag{9}$$

where $\kappa = 2\pi/\Lambda_{\text{bias}}$ and $E_{b0}$ is the peak bias field. Substituting the above into (8) gives the following approximate expression for radiation in the far field:

$$E_\theta(\omega) = \frac{\mu_0 A \cos\theta}{4\pi r} \frac{e\mu_{\text{trans}}(1 - R)}{h\upsilon} W_{\text{opt}} F_s(\omega, \tau_0) E_{b0} \cdot \frac{\sin[Nd(\kappa \pm k(\sin\theta + \sin\alpha))/2]}{2\sin[d(\kappa \pm k(\sin\theta + \sin\alpha))/2]}. \tag{10}$$

When the array is illuminated at normal incidence, four main lobes are expected, one pair inside and one pair outside the semiconductor. In free space, the lobe directions are given approximately by $|\sin\theta_{max}| = \lambda/\Lambda$. By varying the periodicity of the voltage bias, the emission angle of these lobes can be steered continuously over a range from zero to nearly $\pm\pi/2$.

If the array is illuminated at an angle $\alpha$ with respect to the normal, the power pattern is skewed away from its previously symmetric form, and one or two lobes may be suppressed. Fig. 2 shows a calculation of the beam direction $\theta_{max}$ as a function of bias period $\Lambda_{bias}$ for both normal and off-normal incidence.

From (10), the width of the lobe, defined as the angle between the first nulls, is

$$\Delta\theta = \frac{2\lambda}{L\cos\theta_{max}} \tag{11}$$

where $L$ is the array length. Thus, when the radiated beam is steered away from the normal, the beam width increases and the field intensity decreases due to the radiation pattern of the dipole.

### B. Experiment

The layout of a 64 element photoconducting antenna array is shown in Fig. 3. The electrodes, AuGe–Ni deposited on a semiinsulating GaAs substrate, are each 2 mm long and 20 $\mu$m wide, and are spaced 150 $\mu$m apart center to center. They are independently biased by means of slide potentiometers connected to a common voltage supply. The total length of the array is 9.45 mm. Several pieces of GaAs are glued to the back of the array wafer to delay reflections from the semiconductor–air interface, which would interfere with the primary signal. The device described above is a larger version of an earlier array, which consisted of 32 electrodes spaced 100 $\mu$m apart.

Two ultrafast lasers have been used as optical sources. In early experiments, the arrays were pumped with a dual-jet hybridly mode-locked dye laser operating at 640 or 830 nm. Later experiments were done with a self-mode-locked Ti:sapphire laser at 820 nm. Both lasers have pulse widths of less than 200 fs, and generate broad-band radiation extending into the terahertz region of the spectrum.

Radiated electric field waveforms were measured using a correlation technique developed previously [7]. The detector, a photoconducting dipole antenna, consists of a 100 $\mu$m dipole with a 5 $\mu$m photoconductive gap at its feed point. The antenna is gated by a fraction of the laser pulse, which is focussed onto the gap. The photoconductor is radiation-damaged silicon-on-sapphire and has a carrier lifetime of about 600 fs, allowing for rapid measurement of the incident field. A sapphire lens was attached to the dipole to improve its collection efficiency [17]. The field strength as a function of time was obtained by recording the gated output current from the dipole detector while varying the relative time delay between the

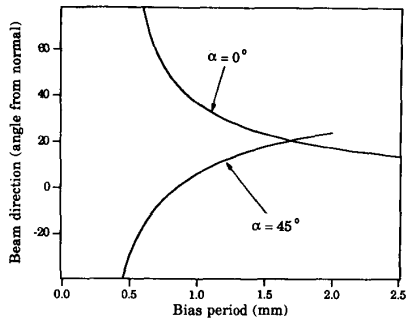


Fig. 2. Theoretical plot of beam direction as a function of bias period for normal incidence of the pump beam ($\alpha = 0$) and $\alpha = 45°$.

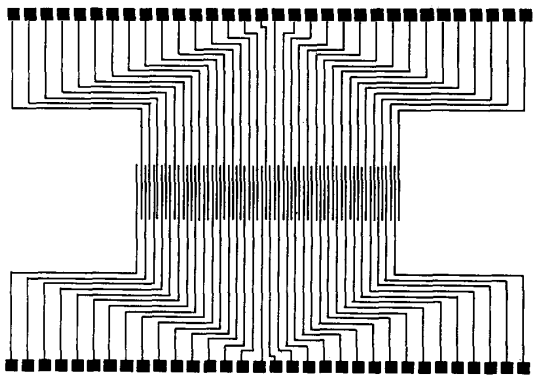

Fig. 3. Photoconducting antenna array with 64 electrodes spaced 150 $\mu$m center to center.

pump pulse, which illuminated the antenna array, and the gating pulse to the detector.

From (10), it is evident that different frequency components produced by the sinusoidally biased array will radiate in different directions. Therefore, in order to be steerable, the radiated beam must be quasi-sinusoidal. To meet this requirement, the spectrum of the radiation emitted by the photoconducting antenna elements was narrowed by illuminating the array with a train of optical pulses rather than a single pulse. The pulse train consisted of either four or seven optical pulses of equal intensity, each spaced 2 ps apart, and was generated by passing a single optical pulse through two or three calcite crystals having birefringent delays of two, four and six picoseconds. This method of illumination enhanced the 500 GHz frequency component of the radiated signal, thereby narrowing its spectrum.

Fig. 4(a) shows the radiated signal from the 64 element array pumped by a train of seven optical pulses at normal incidence. The period of the bias voltages on the array electrodes is 0.75 mm, and the detector is positioned at about 50°, close to the calculated beam direction. Because the radiation from different antenna elements experiences different delay times, the emitted pulse train is broadened in time with respect to the optical pulse train. Fig. 4(a) also shows the calculated time dependence of

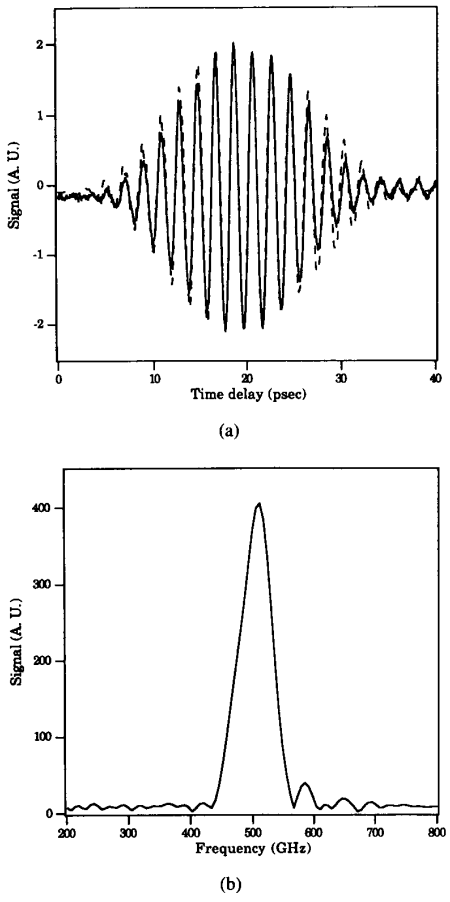


Fig. 4. (a) Waveform detected 4 cm from the array center at an angle of 49° degrees from the normal. The array was illuminated with a train of 7 optical pulses (200 fs pulsewidth) and the bias period was 0.75 mm. Dashed line shows the calculated waveform. In the calculation a photocurrent rise time of 200 fs and an optical beam width of 5 mm were assumed. (b) Spectrum of the detected waveform.

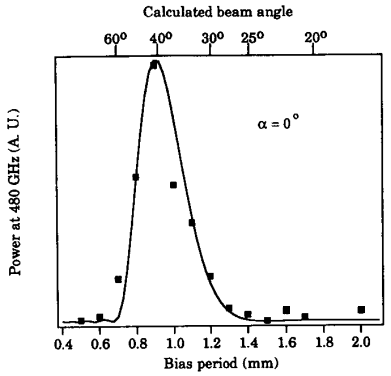


Fig. 5. Power amplitude of the 480 GHz component as a function of bias period, using the 3.2 mm long array illuminated at normal incidence. Markers are data; solid line is the theoretical calculation. Top axis shows the beam direction corresponding to the bais period on the lower axis.

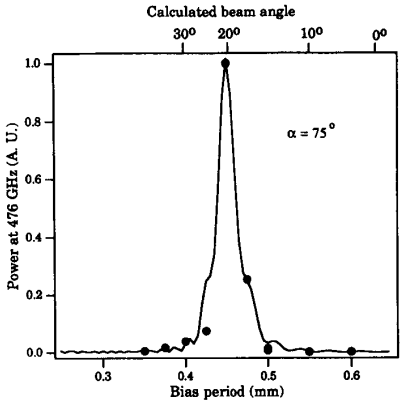


Fig. 6. Power amplitude of the 480 GHz component as a function of bias period, using the 9.5 mm long array illuminated at an angle of 75° with respect to the normal. Markers are data; solid line is the theoretical calculation. Top axis shows the beam direction corresponding to the bias period on the lower axis.

the radiated waveform, based on the simple model for the photocurrent described previously. Fig. 4(b) shows the spectrum of the detected signal, which has a bandwidth of 64 GHz.

To first demonstrate the steerable property of the array, the detector was kept fixed at 45° and the period of the voltage bias on the array was varied to sweep the angle of the emitted beam across the detector. The array used was 3 mm long and was illuminated at normal incidence. The detected signal should reach a maximum when the beam is pointing toward it, then decrease as the beam is steered away. In order to compare the results with the simple single frequency theory, the time traces obtained for each bias period were fourier transformed and the field amplitude at the peak frequency was measured. The detected power at 480 GHz is plotted as a function of bias period in Fig. 5 along with a calculated curve of the field dependence based on (8) and (9). The good agreement between theory and experiment indicates that the beam angle is changing with bias period, as expected.

To study the effect of off-normal illumination on the beam direction, the same experiment was done with the pump beam oriented at 75° to the array normal. The power at 480 GHz is shown in Fig. 6 as a function of bias period, along with the calculated dependence. This data varies more sharply with bias period than the previous data for two reasons. First, a larger array was used, resulting in a narrower beam. Second, off-normal illumination of the array can result in increased sensitivity to bias period, although it does not narrow the beam.

In order to map out the field pattern radiated by the array, the detector rather than the radiated beam had to be moved. To avoid realignment of the gating beam at every position, the beam was coupled into a single-mode optical fiber and a jig was constructed to hold the fiber face flush with the photoconducting gap. The setup is shown in Fig. 7. Dispersion in the 0.4 m length of fiber broadened the optical pulse from 200 fs to an estimated 500 fs. Although the broader gating pulse caused the detector response to roll off sharply after about 300 GHz, and reduced the

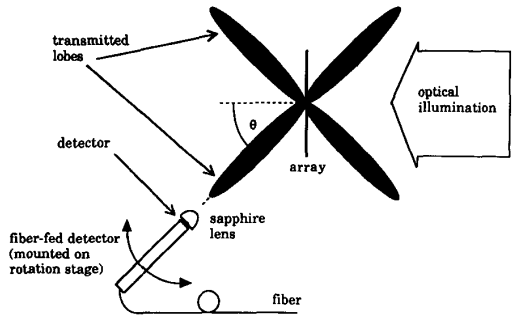


Fig. 7. Experimental setup using the fiber-fed dipole detector and measuring the transmitted lobes of the power pattern.

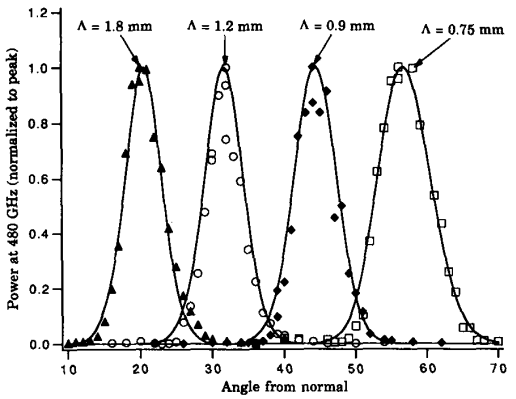


Fig. 8. Power at 480 GHz as a function of detector angle for several bias periods ($\Lambda_{bias}$). Measurements were taken in transmission with the fiber-fed detector approximately 4.5 cm from the array. Solid lines show the theoretical fit, assuming an optical beam width of 6 mm (Gaussian).

overall sensitivity, the 500 GHz component of the signal was still readily detectable. This fiber-fed detector, which is similar to previous work [9], [36] allowed for detailed measurement of the power pattern.

To permit free movement of the detector and jig without blocking the pump beam, the field patterns of the transmitted lobes rather than the reflected lobes were measured, as shown in Fig. 7. Assuming that transmission through the GaAs substrate does not strongly distort the radiated fields, the transmission pattern at normal incidence should be a mirror image of the reflection pattern. The field amplitude was the same order of magnitude for transmission and reflection.

The power at 480 GHz as a function of angle is shown in Fig. 8 for several different bias periods. The beam is clearly being steered away from the normal as the bias period is decreased, and the beam width increases from 6 to 9° as $\theta_{max}$ increases, as expected. A theoretical fit is plotted as a line with each data set. This fit assumes a Gaussian beam diameter of 6 mm. The radiated beam width could be narrowed by increasing the optical beam diameter and the array size.

### C. Power and Efficiency

From (10), the fourier components of the maximum radiated field are given by:

$$E_{max}(\omega, \theta_{max}) = \frac{\mu_0}{4\pi} \frac{A_{\text{array}} \cos\theta_{max}}{r} \frac{(1-R)}{h\upsilon/e} \cdot \left(\frac{P_{opt}}{f_l A_{opt}}\right) \frac{\mu_{\text{trans}} E_{b0}}{2} F_s(\omega) \quad (12)$$

where $P_{opt}$, $A_{opt}$, and $f_l$ are the average laser power, optical beam area, and laser repetition rate, respectively. Generally the optical beam size can be adjusted to overlap the array so that $A_{\text{array}} = A_{opt}$. The maximum intensity of the radiated beam, assuming that it is nearly single frequency, is then

$$I_{max}(\theta_{max}) \cong \frac{1}{\eta_0}\left[\frac{\mu_0}{4\pi} \frac{\cos\theta_{max}}{r} \frac{(1-R)}{h\upsilon/e} \cdot P_{opt} \frac{\mu_{\text{trans}} E_{b0}}{2} F_s(\omega)\right]^2 \frac{2\Delta f}{f_l} \quad (13)$$

where $\eta_0$ is the impedance of free space and $\Delta f$ is the linewidth of the emitted beam.

Up to this point we have considered only the plane of incidence, reducing the array operation to a one-dimensional problem. However, the radiated beam will diffract in two dimensions. The angular beam width in the perpendicular direction is determined by the length of the electrodes $W$, and goes as $\lambda/W$. Taking the beam area as

$$A_{eff} = \frac{\lambda^2 r^2}{A_{\text{array}} \cos\theta_{max}} \quad (14)$$

the radiated power in a single lobe is approximately

$$P_{rad} \cong \frac{1}{\eta_0}\left[\frac{\mu_0}{4\pi} \frac{(1-R)}{h\upsilon/e} P_{opt} \frac{\mu_{\text{trans}} E_{b0}}{2} F_s(\omega)\right]^2 \cdot \frac{\lambda^2 \cos\theta_{max}}{A_{\text{array}}} \frac{2\Delta f}{f_l}. \quad (15)$$

We have measured peak fields on the order of 36 mV/cm, corresponding to radiated powers on the order of a nW.

The electrical power supplied to the array is

$$P_{el} = \frac{(1-R)}{h\upsilon/e} P_{opt} \frac{\mu_{\text{dc}} E_{b0}^2 \tau}{2} \quad (16)$$

where $\tau$ is the carrier lifetime and it is assumed that the dark resistance is very high. Neglecting the optical power, which in our case is less than the electrical power, the

efficiency is:

$$\eta_{eff} \cong \frac{P_{rad}}{P_{el}} = \frac{1}{4\eta_0}\left[\frac{\mu_0}{4\pi}\right]^2 \frac{\mu_{trans}^2}{\mu_{dc}\tau}\frac{\cos\theta_{max}}{A_{array}}\frac{(1-R)}{h\nu/e}$$

$$\cdot P_{opt}F_s^2(\omega)\lambda^2\frac{2\Delta f}{f_l}. \quad (17)$$

Equations (13)–(17) illustrate some general properties. First, since the field is largest and the beam width is smallest near the normal, it is advantageous to scan in the neighborhood of $\theta = 0$. The scanning range can be centered at $\theta = 0$ by illuminating the array at off-normal incidence ($\alpha > 0$). The radiated power can be increased most easily by scaling up the optical power. For pulsed lasers with the same average power, a lower rep rate (higher pulse energy) is preferable. Increasing the field strength will also increase the radiated power, but the maximum field is limited to a few kV/cm to preserve the ohmic current dependence. Finally, reducing the carrier lifetime of the substrate material by radiation damage should benefit the array efficiency since less nonradiative power will be dissipated; however, the radiation damage may also degrade the transient mobility.

## IV. Frequency Tuning

Under excitation by a single subpicosecond optical pulse, the array will generate frequencies ranging from a few GHz to several terahertz. From (10), it is clear that the frequency components will be dispersed by the sinusoidally biased array. The frequency component at a given detection angle $\theta$, and for a pump angle of incidence $\alpha$, is given by:

$$f_{max} = \frac{c}{\Lambda_{bias}(\sin\theta + \sin\alpha)} \quad (18)$$

Thus the frequency content at a given position in the far field can be scanned by changing the bias period $\Lambda_{bias}$.

This property was demonstrated experimentally with the 32 element array, pumped by a single 150 fs pulse at 640 nm. The waveforms are shown in Fig. 9 for bias periods ranging from 2.8 to 0.6 mm and a fixed detector angle of 48°. It is clear from the waveforms that the frequency content is increasing as the bias period is reduced. Fig. 10 plots the peak frequency $f_{max}$ of the waveforms as a function of bias period, along with (18). The tuning range extended from 200 to 800 GHz. Since the maximum frequency is inversely proportional to the element spacing $d$ and the minimum frequency is inversely proportional to the array length $L$, this range could be extended by using a larger array with closely spaced electrodes. The ultimate limit of the tuning range is determined by the frequency content of the radiated field.

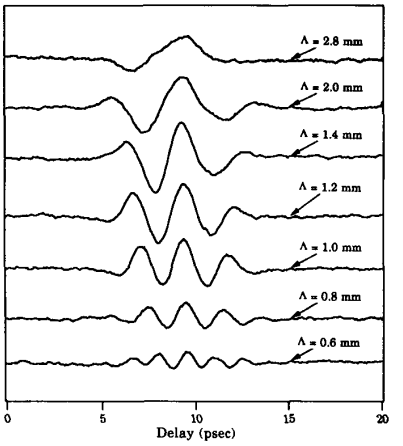


Fig. 9. Waveforms detected at an angle of 48° from the 32 element array illuminated by a single pulse at normal incidence. The frequency content of the waveform changes as the bias period is varied.

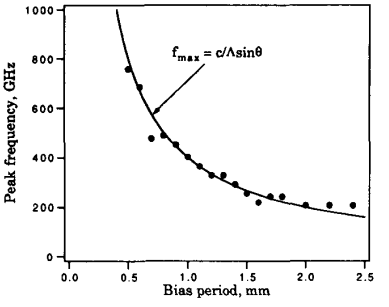


Fig. 10. Peak frequency of the detected waveform as a function of bias period. The solid line is a theoretical fit with $\theta = 48°$.

## V. Spatial-to-Temporal Mapping

The frequency tuning results illustrate a general property of the array under single pulse illumination: the spatial variation of the electric field as a function of position across the array is mapped onto the time dependence of the radiated waveform. In the results discussed above, the sinusoidal spatial profile of the applied electric field created the sinusoidal time dependence of the radiated field.

The spatial to temporal mapping is easily understood by considering the set-up shown in Fig. 11, in which the array is illuminated with a single optical pulse at an angle $\alpha$ with respect to the normal. Since the pump beam travels a different path length to each antenna element, each element radiates at a slightly different time, with the delay given in (3). Similarly, if the detection point is at some angle $\theta$ with respect to the normal, the radiation from each element travels a different path length to the detector, with a corresponding delay given in (2). These position-dependent delays cause the radiative contributions from each element in the array to be staggered in time. Since the strength of each contribution is proportional to the bias on

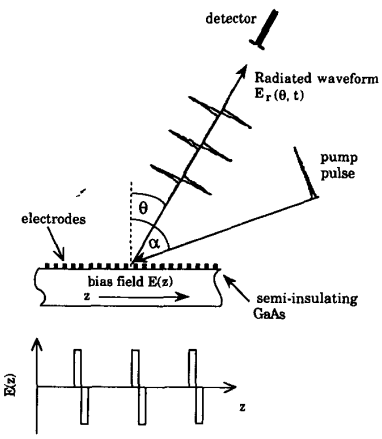


Fig. 11. Experimental layout. When the array is illuminated by a short laser pulse, it generates a burst of nondirectional, broad-band electromagnetic radiation. The spatial profile of the electric field on the array is mapped onto the time dependence of the radiated waveform.

the element, the spatial profile of the electric field on the array is mapped onto the temporal waveform.

This property is easily shown mathematically. We replace the summation in (6) with an integral to get

$$E_\theta(r, \theta, t) = \frac{\mu_0 \cos\theta}{4\pi r} \frac{\partial}{\partial t} \int_{S'} E_b'(z') \cdot \sigma_s\left(t - \frac{z'}{c}(\sin\theta + \sin\alpha)\right) ds' \quad (19)$$

where $S'$ is the emitting area, $E_b(z')$ is the bias field as a function of position, and $\sigma_s(t)$ is the transient surface photoconductivity. For a short (100 fs) pulse at 830 nm, Monte-Carlo calculations indicate that the rise time of the injected carrier velocity is on the order of a few hundred femtoseconds [35]. Therefore, the transient photoconductivity may be roughly approximated by a step function, giving:

$$\sigma_s(t) = N_s e \mu_{\text{trans}} U(t) \quad (20)$$

where $N_s$ is number of carriers per unit area injected by the laser pulse and $U(t)$ is the step function. Substituting (20) into (19) and taking the time derivative inside the spatial integral transforms the step function of a delta function. The final expression for the radiated field is then

$$E_{rad}(r, \theta, t) = \frac{\mu_0}{4\pi} \frac{We\mu_{\text{trans}} N_s \cos\theta}{r} \frac{c}{\sin\theta + \sin\alpha} \cdot E_b\left(z' = \frac{c(t - t_0)}{\sin\theta + \sin\alpha}\right) \quad (21)$$

where $t_o$ is the average propagation delay. Thus the spatial profile of the applied dc field is translated into the temporal profile of the radiated field as expected. While the radiation emitted from the array is no longer directional, the detection angle is still important because it determines the scaling of the spatial to temporal mapping.

If the radiation is produced by optical rectification, the rise time will still be very fast, but the fall time will no longer follow the slowly decaying carrier density. The results do not simplify as neatly, but the mapping property is essentially the same.

## VI. Multiplexing

The mapping property of the array was used to convert parallel electronic data into a series of electromagnetic pulses radiated into free space. A specific pulse shape was chosen to represent a one, while the absence of this pattern in the expected interval represented a zero. The electronic data was encoded by biasing the array electrodes to produce the desired spatial pattern of zeros and ones, and the multiplexing was achieved by the radiation process.

The pump pulse was incident on the array at an angle of about 70° relative to the normal. At this angle, the beam, which has a nominal diameter of 3 mm, illuminated nearly the full length of the 9.5 mm long array. The detector was placed at an angle of about 25° relative to the normal.

The bias voltages applied to the electrodes in the illuminated region of the array were selected to produce an electric field with the spatial profile shown in Fig. 12(a). The maximum electric field was roughly 4 kV/cm. Each of the four identical patterns corresponds to a "one," so that the bias across the entire array makes up a four-bit word containing four "ones." Fig. 12(b) shows the expected profile of the radiated waveform, obtained from simulation, using the approach described previously. Fig. 12(c) shows the measured waveform. The spatial bias field is clearly mapped onto the radiated waveform, as expected, and the pattern of ones stored in the dc electric field is converted into a sequence of radiated pulses. This particular spatial pattern was used to represent a one because it was found experimentally to give the strongest and fastest signal. Due to the limited frequency response of the detector, however, the duration of each temporal "one" is still several picoseconds, much longer than the predicted duration. There is also some variation in the amplitude of the peaks, which is caused by the spatial Gaussian profile of the illuminating pulse. Fig. 13 shows several waveforms in which some of the spatially encoded "ones" shown above were removed to encode to zero. Again, the spatial bias pattern is mapped onto the waveform for any arbitrary four-bit word. For a given bit rate, the number of bits per word should scale with the available optical power, since the maximum duration of the waveform is proportional to the illuminated length of the array.

The major advantage of the array time-division multiplexer is its high speed. Given a fast enough detector, the peak bit rate could be increased to a terahertz or more. Recent experiments have shown that the pulses emitted by subpicosecond optical excitation at semiconductor surfaces are as short as 160 fs, with spectral content out to 4 THz [16]. However, the bias field in these experiments was probably much higher than the fields used in the ar-

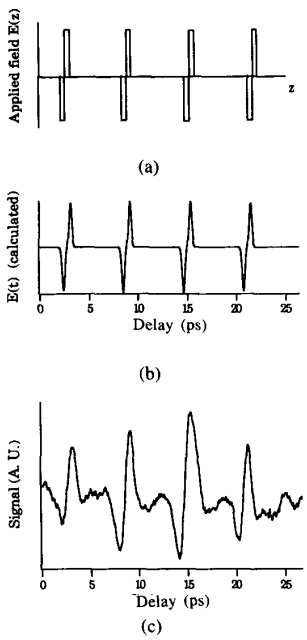


Fig. 12. (a) Spatial profile of the electric field in the semiconductor, which is controlled by the voltages applied to the electrodes. Each of the four identical patterns represents a one. (b) Calculated time dependence of the radiated waveform, obtained by simulation. (c) Measured time dependence of the radiated waveform (electric field amplitude).

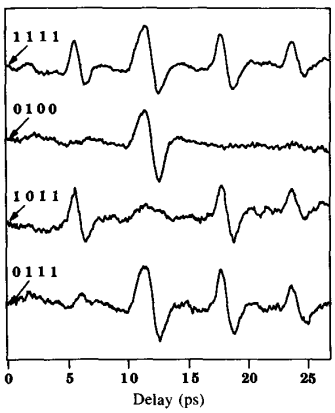


Fig. 13. Radiated waveforms, corresponding to various combinations of zeros and ones, which are encoded by the applied dc electric field.

ray, which are limited to a few kV/cm to insure that the current–voltage relationship is ohmic. At lower fields, the radiated pulses seem to be considerably broader.

Given sufficient optical power, the data generated by a photoconducting antenna array could conceivably be demultiplexed by a second array made of a fast photoconducting material such as radiation-damaged silicon-on-sapphire. Each pair of electrodes on the array would act as a detector, in which photocurrent would flow only when an optical clock pulse coincided with a radiated pulse representing a one. The detectors would be positioned on the demultiplexing device so that the arrival of the clock pulse at each detector overlapped with a single time slot. The nondirectional nature of the radiation produced by the array in this mode results in low radiated intensities, posing a practical limitation to this technique. Nonetheless, demultiplexing would be feasible with careful design and an amplified subpicosecond laser system.

## VII. Discussion

In all of the experiments described above, the power radiated by the array is low, and it would have to be scaled up for practical applications. For moderate optical pulse energies, the peak power is proportional to the square of the optical fluence, and could be substantially increased using an amplified subpicosecond laser. The saturation of radiated power at high optical fluences has been observed and studied in other kinds of photoconducting antennas. For radiation from semiconductor surfaces pumped with a 10 Hz laser system [25], it was found that the radiated intensity was directly proportional to the optical fluence, rather than its square, for fluences above $10^{-6}$ J/cm$^2$. The nonlinear behavior was attributed to carrier screening of the field. For large aperture photoconducting antennas in the near field [37], a nonlinear dependence of the radiated signal on optical fluence was found to begin around $10^{-4}$ J/cm$^2$. Since the experiments discussed in this paper were done with fluences of only 10 nJ/cm$^2$, there is clearly room to scale up the optical pump power.

Another practical consideration is the bandwidth of the radiated signal. The power spectrum emitted by the array under pulse train illumination was measured to be about 80 GHz, broad enough so that dispersion would prevent efficient collection of the radiated power. The power bandwidth is inversely proportional to the duration of the pulse train, and could be readily reduced by increasing the number of pulses. The same goal could be achieved with optical heterodyning techniques, which have recently been used to generate free-space radiation at 60 GHz from HEMT's [38]. With the rapid progress currently being made in mode-locking laser diodes, heterodyning may not be necessary. The 350 GHz monolithic CPM lasers recently demonstrated by Wu *et al.* [39] are especially promising although relatively low-power at present.

The array may also be designed for beamsteering at millimeter-wave frequencies, which are of interest in radar applications because of transmission windows in the atmosphere. Longer wavelengths would require larger arrays to maintain the same beam width and scanning range. However, the radiation efficiency in this frequency range may benefit from increased carrier mobility.

In the experiments above, relatively high voltages were required across the 100–150 $\mu$m electrode spacings in order to generate a high electric field and considerable electrical power is dissipated by nonradiative current flow. If p–i–n junctions were used as the emitters, the same field magnitude could be achieved with only a few volts bias and the power requirements could be substantially reduced. For a vertical p–i–n structure, the current elements

would be normal to the semiconductor surface rather than parallel. Therefore, the dipole pattern would be strongest at off-normal angles and the radiation pattern of the array would have a sine dependence instead of the cosine dependence described here. Also, since the p–i–n structures must be reverse biased, the field distribution along the array would have a nonzero component. Despite these differences, a p–i–n array is very feasible, and the reduced voltage requirement would make the array a more practical device.

In the paper reported here, the strength of the antenna elements has been controlled by the applied field, while the optical illumination remains constant with respect to position. The same effect can be produced using a constant bias field and patterning the optical illuminations [40]. In principle a liquid crystal array could be used as the mask, permitting electrical control. As in the case of a p–i–n array, there would be a nonzero component to the strength of the radiating elements. This approach would lend itself to two-dimensional arrays.

In conclusion, we have discussed the generation of electrically controlled submillimeter wave pulses by a photoconducting antenna array and have presented experimental results which demonstrate its properties.

## Acknowledgment

We would like to acknowledge the assistance of W. Xin in sample preparation and of C. Huddle in constructing the fiber-fed detector.

## References

[1] B. B. Hu, X.-C. Zhang, D. H. Auston, and P. R. Smith, "Free-space radiation from electro-optic crystals," *Appl. Phys. Lett.*, vol. 56, pp. 506–508, Feb. 5, 1990; C. Fattinger and D. R. Grischkowksy, "A Cherenkov source for freely-propagating terahertz beams," *IEEE J. Quantum Electron.*, vol. 25, pp. 2608–2610, Dec. 1989.

[2] G. Mourou, C. V. Stancampiano, and D. Blumenthal, "Picosecond microwave pulse generation," *Appl. Phys. Lett.*, vol. 38, pp. 470–472, Mar. 15, 1981; G. Mourou, C. V. Stancampiano, A. Antonetti, and A. Orszag, "Picosecond microwave pulses generated with a subpicosecond laser-driven semiconductor switch," *Appl. Phys. Lett.*, vol. 39, pp. 295–297, Aug. 15, 1981.

[3] R. Heidemann, T. Pfeiffer, and D. Jager, "Optoelectronically pulsed slot-line antennas," *Electron. Lett.*, vol. 19, pp. 316–317, Apr. 28, 1983.

[4] D. H. Auston, K. P. Cheung, and P. R. Smith, "Picosecond photoconducting hertzian dipoles," *Appl. Phys. Lett.*, vol. 45, pp. 284–286, Aug. 1, 1984.

[5] A. P. DeFonzo, M. Jarwala, and C. R. Lutz, "Transient response of planar integrated optoelectronic antennas," *Appl. Phys. Lett.*, vol. 50, pp. 1155–1157, Apr. 27, 1987; A. P. DeFonzo and C. R. Lutz, "Optoelectronic transmission and reception of ultrashort electrical pulses," *Appl. Phys. Lett.*, vol. 51, pp. 212–214, July 27, 1987.

[6] Y. Pastol, G. Arjavalingam, J.-M. Halbout, and G. V. Kopsay, "Characterisation of an optoelectronically pulsed broadband microwave antenna," *Electron. Lett.*, vol. 24, pp. 1318–1319, October 13, 1988.

[7] P. R. Smith, D. H. Auston, and M. C. Nuss, "Subpicosecond photoconducting dipole antennas," *IEEE J. Quantum Electron.*, vol. 24, pp. 255–260, Feb. 1988.

[8] M. van Exter, C. Fattinger, and D. Grischkowsky, "High-brightness terahertz beams characterized with an ultrafast detector," *Appl. Phys. Lett.*, vol. 55, pp. 337–339, July 24, 1989.

[9] Y. Pastol, G. Arjavalingam, and J.-M. Halbout, "Characterisation of an optoelectronically pulsed equiangular spiral antenna," *Electron. Lett.*, vol. 26, pp. 133–134, Jan. 18, 1990.

[10] D. R. Dykaar, B. I. Greene, J. F. Federici, A. F. J. Levi, L. N. Pfeiffer, and R. F. Kopf, "Log-periodic antennas for pulsed terahertz radiation," *Appl. Phys. Lett.*, vol. 59, pp. 262–264, July 15, 1991.

[11] C. Fattinger and D. Grischkowsky, "Point source terahertz optics," *Appl. Phys. Lett.*, vol. 53, pp. 1480–1482, Oct. 17, 1988.

[12] B. B. Hu, J. T. Darrow, X.-C. Zhang, and D. H. Auston, "Optically steerable photoconducting antennas," *Appl. Phys. Lett.*, vol. 56, pp. 886–888, Mar. 5, 1990; J. T. Darrow, B. B. Hu, X.-C. Zhang, and D. H. Auston, "Subpicosecond electromagnetic pulses from large-aperture photoconducting antennas," *Opt. Lett.*, vol. 15, pp. 323–325, Mar. 5, 1990.

[13] N. Katzenellenbogen and D. Grischkowsky, "Efficient generation of 380 fs pulses of THz radiation by ultrafast laser pulse excitation of a biased metal-semiconductor interface," *Appl. Phys. Lett.*, vol. 58, pp. 222–224, Jan. 21, 1991; —, "Optoelectronic generation of 380 fsec pulses of THz radiation," in *Proc. Picosecond Electronics and Optoelectronics*, 1991. Washington, DC: Opt. Soc. Amer., 1991; S. E. Ralph and D. Grischkowsky, "Trap-enhanced electric fields in semi-insulators: The role of electrical and optical carrier injection," *Appl. Phys. Lett.*, vol. 59, pp. 1972–1974, Oct. 14, 1991.

[14] X.-C. Zhang, B. B. Hu, J. T. Darrow, and D. H. Auston, "Generation of femtosecond electromagnetic pulses from semiconductor surfaces," *Appl. Phys. Lett.*, vol. 56, pp. 1011–1013, Mar. 12, 1990; X.-C. Zhang, J. T. Darrow, B. B. Hu, D. H. Auston, M. T. Schmidt, P. Tham, and E. S. Yang, "Optically induced electromagnetic radiation from semiconductor surfaces," *Appl. Phys. Lett.*, vol. 56, pp. 2228–2230, May 28, 1990; B. B. Hu, X.-C. Zhang, and D. H. Auston, "Temperature dependence of femtosecond electromagnetic radiation from semiconductor surfaces," *Appl. Phys. Lett.*, vol. 57, pp. 2629–2631, Dec. 17, 1990.

[15] L. Xu, X.-C. Zhang, D. H. Auston, and B. Jalali, "Terahertz radiation from large aperture Si p–i–n diodes," *Appl. Phys. Lett.*, vol. 59, pp. 3357–3359, Dec. 23, 1991.

[16] B. I. Greene, J. F. Federici, D. R. Dykaar, R. R. Jones, and P. H. Bucksbaum, "Interferometric characterization of 160 fs far-infrared light pusles," *Appl. Phys. Lett.*, vol. 59, pp. 893–895, Aug. 19, 1991.

[17] C. Fattinger and D. Grischkowsky, "Terahertz beams," *Appl. Phys Lett.*, vol. 54, pp. 490–492, Feb. 6, 1989; —, "Beams of terahertz electromagnetic pulses," in *Proc. Picosecond Electronics and Optoelectronics*, 1989. Washington, DC: Opt. Soc. Amer., 1989, p. 225; M. van Exter and D. R. Grischkowsky, "Characterization of an optoelectronic terahertz beam system," *IEEE Trans. Microwave Theory Tech.*, vol. 38, pp. 1684–1691, Nov. 1990.

[18] Y. Pastol, G. Arjavalingam, J.-M. Halbout, and G. V. Kopsay, "Coherent broadband microwave spectroscopy using picosecond optoelectronic antennas," *Appl. Phys. Lett.*, vol. 54, pp. 307–309, Jan. 23, 1989; Y. Pastol, G. Arjavalingam, J.-M. Halbout, and G. V. Kopsay, "Absorption and dispersion of low-loss dielectrics measured with microwave transient radiation," *Electron. Lett.*, vol. 25, pp. 523–524, Apr. 13, 1989; Y. Pastol, G. Arjavalingam, G. V. Kopsay, and J.-M. Halbout, "Dielectric properties of uniaxial crystals measured with optoelectronically generated microwave transient radiation," *Appl. Phys. Lett.*, vol. 55, pp. 2277–2279, Nov. 27, 1989; G. Arjavalingam, N. Theophilou, Y. Pastol, G. V. Kopsay, and M. Angelopoulos, "Anisotropic conductivity in stretch-oriented polymers measured with coherent microwave transient spectroscopy," *J. Chem. Phys.*, vol. 93, pp. 6–9, July 1, 1990.

[19] D. Grischkowsky, S. Keiding, M. van Exter, and Ch. Fattinger, "Far-infrared time-domain spectroscopy with terahertz beams of dielectrics and semiconductors," *J. Opt. Soc. Amer. B*, vol. 7, pp. 2006–2015, Oct. 1990.

[20] M. van Exter and D. Grischkowsky, "Optical and electronic properties of doped silicon from 0.1 to 2 THz," *Appl. Phys. Lett.*, vol. 56, pp. 1694–1696, Apr. 23, 1990; —, "Carrier dynamics of electrons and holes in moderately doped silicon," *Phys. Rev. B*, vol. 41, pp. 12140–12149, June 15, 1990.

[21] D. Grischkowsky and S. Keiding, "THz time-domain spectroscopy of high Tc substrates," *Appl. Phys. Lett.*, vol. 57, pp. 1055–1057, Sept. 3, 1990.

[22] H. Roskos, M. C. Nuss, J. Shah, B. Tell, and J. Cunningham, "Terahertz absorption between split subbands in coupled quantum wells," in *Picosecond Electronics and Optoelectronics*, vol. 4, T. C. L. G. Sollner and J. Shah, Eds. Washington, DC: Opt. Soc. Amer., 1991.

[23] M. C. Nuss, K. W. Goossen, J. P. Gordon, P. M. Mankiewich, and M. L. O'Malley, "Terahertz Time-domain measurement of the conductivity and superconducting bandgap in Niobium," *J. Appl. Phys.*, vol. 70, pp. 2238–2241, Aug. 15, 1991.

[24] M. C. Nuss, K. W. Goossen, P. M. Mankiewich, and M. L. O'Malley, "Terahertz surface impedance of thin $YBa_2Cu_3O_7$ superconducting films," *Appl. Phys. Lett.*, vol. 58, pp. 2561–2563, June 3, 1991; M. C. Nuss, P. M. Mankiewich, M. L. O'Malley, E. H. Westerwick, and P. B. Littlewood, "Dynamic conductivity and coherence peak in $YBa_2Cu_3O_7$ Superconductors," *Phys. Rev. Lett.*, vol. 66, pp. 3305–3308, June 24, 1991.

[25] B. I. Greene, J. F. Federici, D. R. Dykaar, A. F. J. Levi, and L. Pfeiffer, "Picosecond pump and probe spectroscopy utilizing freely propagating terahertz radiation," *Opt. Lett.*, vol. 16, p. 48, Jan. 1, 1991.

[26] L. Xu, X.-C. Zhang, D. H. Auston, and W. I. Wang, "Internal piezoelectric fields in GaInSb/InAs strained-layer superlattices probed by optically induced microwave radiation," *Appl. Phys. Lett.*, vol. 59, pp. 3562–3564, Dec. 30, 1991.

[27] B. B. Hu, X.-C. Zhang, and D. H. Auston, "Terahertz radiation induced by subband-gap femtosecond optical excitation of GaAs," *Phys. Rev. Lett.*, vol. 67, pp. 2709–2711, Nov. 4, 1991.

[28] For a review, see, for example, "Optoelectronic signal processing for phased array antennas," *Proc. SPIE*, K. B. Bhasin and B. M. Hendrickson, Eds., vol. 886, 1988.

[29] G. J. Simonis and K. G. Purchase, "Optical generation, distribution, and control of microwaves using laser heterodyne," *IEEE Trans. Microwave Theory Tech.*, vol. MTT-38, pp. 667–669, May 1990.

[30] N. Froberg, M. Mack, B. B. Hu, X.-C. Zhang, and D. H. Auston, "500 GHz electrically steerable photoconducting antenna array," *Appl. Phys. Lett.*, vol. 58, pp. 446–448, Feb. 4, 1991.

[31] B. B. Hu, N. Froberg, M. Mack, X.-C. Zhang, and D. H. Auston, "Electrically controlled frequency scanning by a photoconducting antenna array," *Appl. Phys. Lett.*, vol. 58, pp. 1369–1371, Apr. 1, 1991.

[32] N. M. Froberg, B. B. Hu, X.-C. Zhang, and D. H. Auston, "Time-division multiplexing by a photoconducting antenna array," *Appl. Phys. Lett.*, vol. 59, pp. 3207–3209, Dec. 16, 1991.

[33] J. D. Kraus, *Antennas*, Second Ed. New York: McGraw-Hill, 1988, chs. 4 and 11.

[34] S. L. Chuang, S. Schmitt-Rink, B. I. Greene, P. N. Saeta, and A. F. J. Levi, "Optical rectification at semiconductor surfaces," *Phys. Rev. Lett.*, vol. 68, pp. 102–106, Jan. 6, 1992.

[35] G. M. Wysin, D. L. Smith, and A. Redondo, "Picosecond response of photoexcited GaAs in a uniform electric field by Monte Carlo dynamics," *Phys. Rev. B*, vol. 38, pp. 12514–12524, Dec. 15, 198.

[36] C. R. Lutz and A. P. DeFonzo, "Far field characteristics of optically pulsed millimeter wave antennas," *Appl. Phys. Lett.*, vol. 54, pp. 2186–2188, May 29, 1989.

[37] J. T. Darrow, X.-C. Zhang, and D. H. Auston, "Power scaling of large-aperture photoconducting antennas," *Appl. Phys. Lett.*, vol. 58, pp. 25–28, Jan. 7, 1991; J. T. Darrow, X.-C. Zhang, D. H. Auston, and J. D. Morse, "Saturation properties of large-aperture photoconducting antennas," *IEEE J. Quantum Electron.*, vol. 28, pp. 1607–1616, June 1992.

[38] D. V. Plant, D. C. Scott, H. R. Fetterman, L. K. Shaw, W. Jones, and K. L. Tan, "Optically generated at 60 GHz millimeter waves using AlGaAs/InGaAs HEMT's integrated with both quasi-optical antenna circuits and MMIC's," *IEEE Photon. Technol. Lett.*, vol. 4, Jan. 1992.

[39] Y. K. Chen, M. C. Wu, T. Tanbun-Ek, R. A. Logan, and M. A. Chin, "Subpicosecond monolithic colliding-pulse mode-locked multiple quantum well lasers," *Appl. Phys. Lett.*, vol. 58, pp. 1253–1255, Mar. 25, 1991.

[40] X.-C. Zhang and D. H. Auston, "Generation of steerable submillimeter waves from semiconductor surfaces by spatial light modulators," *Appl. Phys. Lett.*, vol. 59, pp. 768–770, Aug. 12, 1991.

**Nan Moore Froberg** received a B.S.E. in mechanical engineering from Princeton University, Princeton, NJ, in 1985. In 1989 she received the M.S. degree in electrical engineering from Columbia University, New York, NY.

From 1985 to 1987 she worked on laser diagnostics for combustion systems at United Technologies Research Center. Currently, she is pursuing the Ph.D. degree. Her research involves the generation of electromagnetic transients by ultrashort optical pulses.

**Bin Bin Hu,** photograph and biography not available at the time of publication.

**Xi-Cheng Zhang,** for a photograph and biography, see p. 1616 of the June 1992 issue of this JOURNAL.

**David H. Auston** (S'67–M'69–SM'87–F'89), for a photograph and biography, see p. 1616 of the June 1992 issue of this JOURNAL.